Supplementary Information

Analytical measurements

Determination of the CDOM spectral absorption coefficient

Absorption spectra were determined using a UV-visible spectrophotometer (UV-2550 bi-channel; Shimadzu, Tokyo, Japan) equipped with two 10 cm path-length quartz cuvettes. Sample absorbance was automatically corrected for the absorbance of Milli-Q water. Absorbance scans ranged from 200 to 800 nm, with a spectral resolution of 1 nm. The absorption coefficient of CDOM was calculated according to equation (1):

$$a(\gamma) = 2.303\,A(\lambda)/l \quad (1)$$

where, A(λ) is the absorbance at wavelength λ; and r is the path length of the quartz cuvette in meters.

The spectral slope of the CDOM absorption curve (S) was calculated according to a non-linear regression over the 275–500 nm wavelength range, according to:

$$\alpha(\lambda) = \alpha(\lambda_0)\exp[S(\lambda_0—\lambda)]+K \quad (2)$$

where, $\alpha(\lambda)$ is the absorption coefficient at wavelength λ; $\alpha(\lambda_0)$ is the absorption at the reference wavelength λ_0 of 440 nm; S is the spectral slope; and K is a background parameter that accounts for baseline shifts or attenuation due to factors other than CDOM. S was measured in the wavelength ranges of 275–295 nm ($S_{275\text{-}295}$, nm^{-1}) and 350–400 nm ($S_{350\text{-}400}$, nm^{-1}). $S_{275\text{-}295}$ is used to characterize DOM, with low values generally indicative of high-molecular-weight DOM that are linked to photochemical modification (Helms et al., 2008; Ortega-Retuerta et al., 2009). The spectral slope ratio (S_R) was defined as the ratio of the two spectral slopes, $S_{275\text{-}295}$ to $S_{350\text{-}400}$. S_R is also a sensitive indicator of photochemically induced changes in the molecular weight within the CDOM pool, with increases in S_R suggesting stronger photodegradation (Ortega-Retuerta et al., 2009; Spencer et al., 2009). The absorption coefficient at 254 nm (a(254)), the absorption of light at 254 nm per unit of carbon, was used to quantify CDOM abundance. The specific UV absorbance ($SUVA_{254}$) can be

used to measure aromaticity (Weishaar et al., 2003; Massicotte et al., 2017) and molecular weight (Chowdhury, 2013) of DOM, with higher values generally indicative of higher aromaticity.

EEMs and determination of the CDOM fluorescence index

EEMs fluorescence spectra were obtained using a F-4500 fluorescence spectrophotometer with a 1 cm quartz cuvette (Shimadzu) (Hoge et al., 1993). The emission spectra were scanned every 5 nm from 250 nm to 550 nm, and at the excitation wavelengths between 200–400 nm at 5 nm intervals, with 5 nm slit widths for the excitation and emission modes. The FL Toolbox, which was developed by Wade Sheldon (University of Georgia) for MATLAB, was used to remove the Rayleigh and Raman scattering peaks using the Delaunay triangulation method (Zepp et al., 2004). The fluorescence intensities of the samples were corrected with Milli-Q water blank EEMs and then normalized to the water Raman integrated area maximum fluorescence intensities (Ex/Em = 350 nm/365–430 nm, 5 nm bandpass) (Singh et al., 2010). Raman units (RU) (Stedmon et al., 2007; Singh et al., 2010) were used as the units for the Raman peak areas of water when the excitation wavelength of 350 nm was used for correction. EEMs were modeled using PARAFAC in MATLAB 7.5 with the DOMFluor toolbox (Stedmon and Bro, 2008).

$$X_{ijk} = \sum_{n=1}^{F} a_{in} b_{jn} c_{kn} + \varepsilon_{ijk} \qquad (3)$$

where X_{ijk} is the fluorescence intensity of the *i*th sample at the *k*th excitation and *j*th emission wavelengths; a_{in} is directly proportional to the concentration (scores) of the nth fluorophore in the *i*th sample; b_{jh} and c_{kn} are the estimates of the emission and excitation spectra (loadings) of the nth fluorophore at wavelengths *j* and *k*, respectively; *F* is the number of components (fluorophores); and ε_{ijk} represents the unexplained variability of the model (Singh et al., 2010). Split-half analysis validation was used to determine the number of fluorescent components. The fluorescence intensity of each fluorescent component was evaluated (Fig. 3, Table S1).

Determination of DOC, chlorophyll-a, heterotrophic bacterial abundance, dissolved oxygen, and other parameters

Concentrations of DOC were determined using the Shimadzu TOC-V_{CPH} total organic carbon analyzer with an injection volume of 80 μL. The accuracy of the test was ensured by measuring a deep seawater reference (Hansell Laboratory, University of Miami) every 10 samples. For Chl-a analysis, 200 mL subsamples were filtered through 0.7 μm GF/F filters (Whatman, U.S.A.), which were then stored in the dark at 20 ℃ until analysis. The Chl-a was extracted in 90% acetone and centrifuged for 10 min at 4 ℃ before being measured with a fluorescence spectrophotometer (7200-000, Turner Designs, CA) according to the method from Parsons et al. (1984). Dissolved oxygen (DO) was determined by iodination using the Winkler titration method (Carpenter, 1964), the endpoint was determined using starch as a visual indicator.

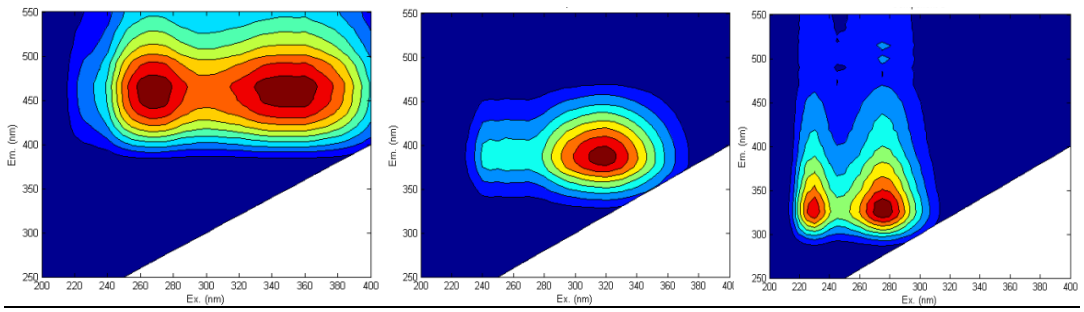

Fig. S1. Representative fluorescence excitation-emission matrix spectra (EEM) contours from samples in the ECS and the YS during winter. The fluorescence intensities were quantified using Raman units (nm^{-1}).

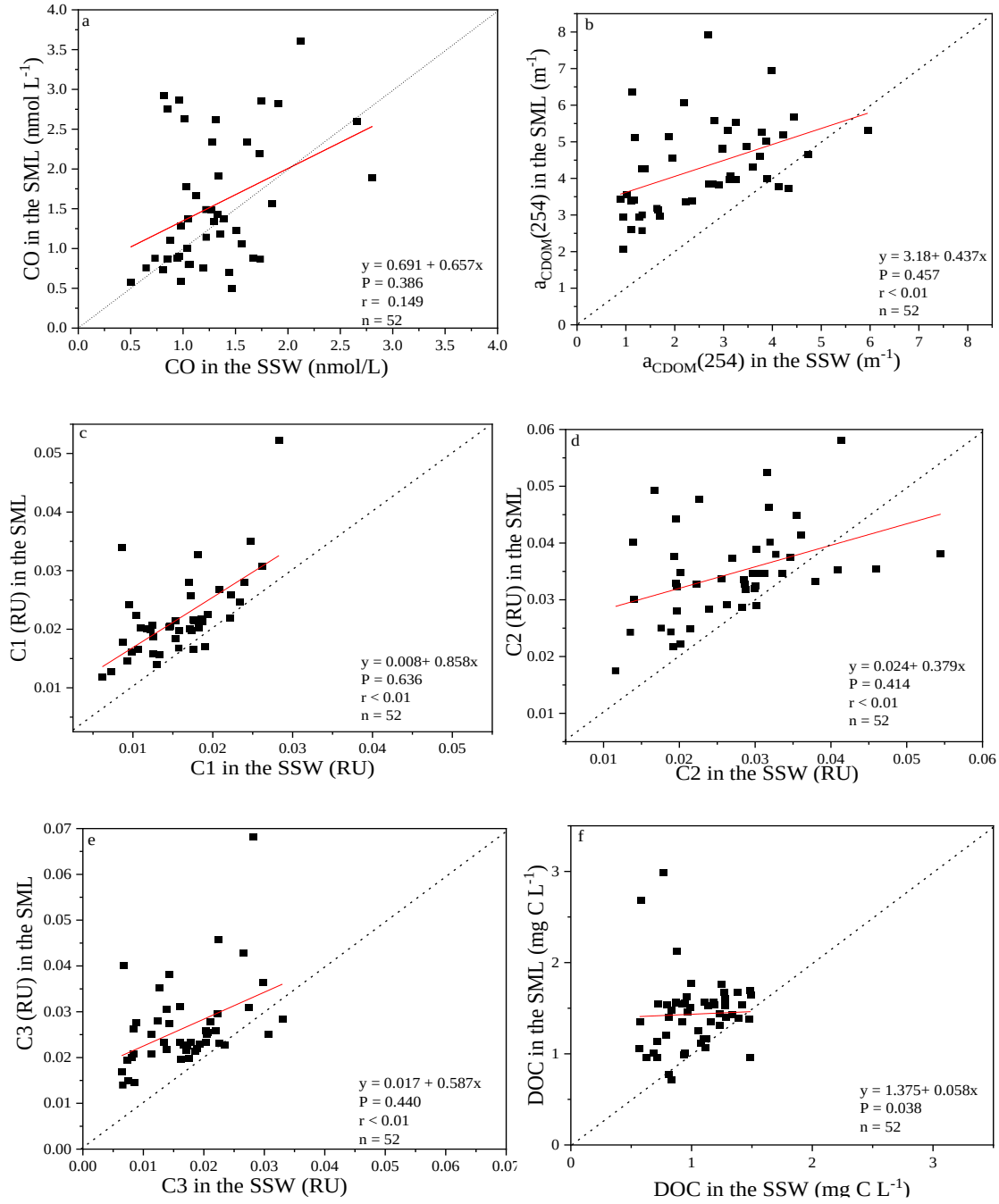

Fig. S2. Correlations between the microlayer CO, CDOM, DOC, and three fluorescence components, as well as their sub-surface water concentrations in winter. The dashed lines correspond to the 1:1 lines, and the full lines are the regression models.

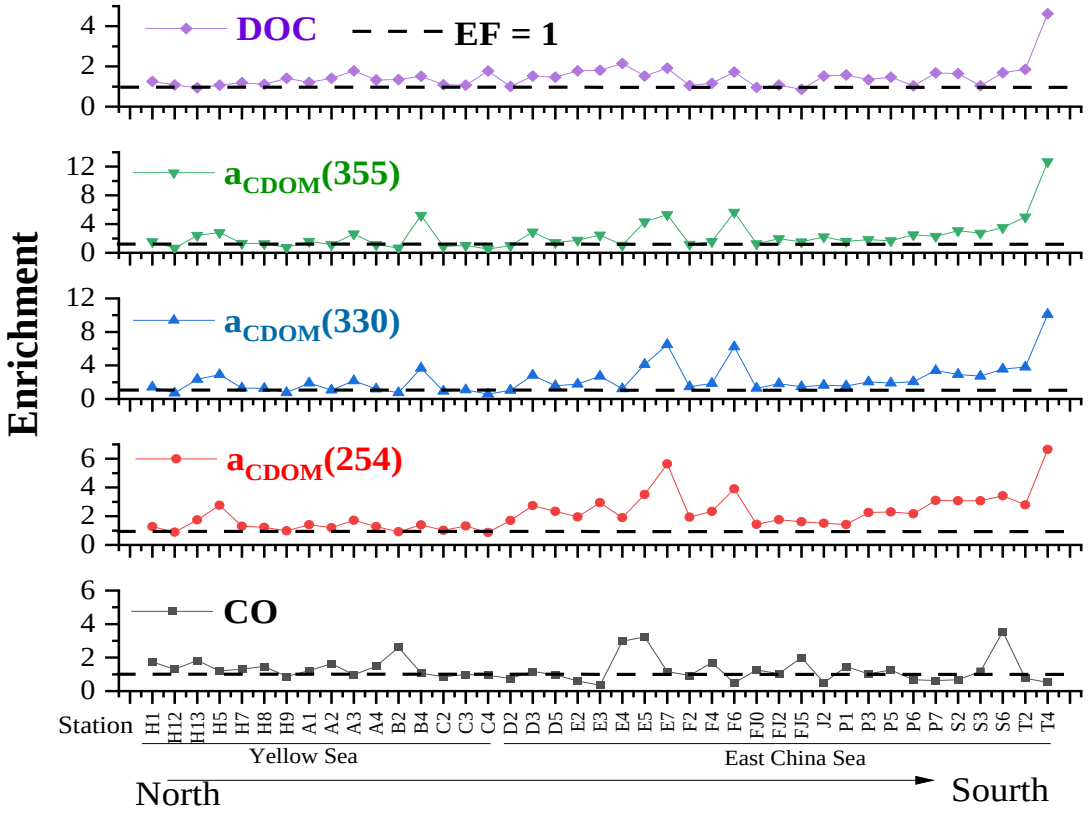

Fig. S3. EFs of CDOM absorption, DOC, and CO in the SML at different stations.

Table S1. Location, local time, depth, temperature, salinity, wind speed and net radiation conditions of SML and SSW water sampling.

Station	Time	Longitude	Latitude	Depth (m)	Temperature (℃)	Salinity	Wind speed (m/s)	Net radiation
A1	5:25	121.25	35.98	34	8.29	32.18	5.91	-103.9
A2	9:45	122.15	35.98	43	10.12	31.97	1.53	147.9
A3	14:16	123.05	35.98	69	11.27	32.25	2.78	50.6
A4	19:01	123.97	35.98	74	10.25	32.25	3.25	-52.3
B1	22:35	120.51	35.00	27	10.15	31.72	3.15	-77.3
B2	18:07	121.35	35.00	33	11.11	31.83	3.40	-55.6
B3	13:34	122.20	35.00	52	11.77	32.09	7.67	187.3
B4	8:42	123.06	35.00	67	11.51	32.35	8.82	32.3
B5	2:22	123.98	35.00	78	11.09	32.41	10.05	-42.4
C1	5:02	121.25	34.00	12	8.69	31.10	7.29	-86.8
C2	9:33	122.14	34.00	17	10.93	31.66	4.27	85.6
C3	14:19	123.05	34.00	66	12.30	32.42	3.67	2. 7
C4	19:11	124.00	34.00	75	12.67	32.83	7.53	-38.6
D1	17:11	122.49	31.36	18	10.90	31.22	8.66	-15.4
D2	19:09	122.49	31.60	22	10.15	31.13	6.91	-23.7
D3	22:50	122.99	31.90	32	14.01	32.94	5.32	-28.1
D4	3:19	123.50	32.15	35	13.46	32.44	6.84	-27.4
D5	6:05	124.00	32.45	36	13.43	32.28	7.92	-32.9
E1	1:58	122.31	29.36	12	13.64	28.85	4.03	-82.8
E2	22:22	122.61	29.11	48	16.56	33.30	6.53	-15.2
E3	18:17	123.01	28.83	63	18.40	34.01	2.08	-20.5
E4	13:34	123.57	28.48	70	18.99	34.22	3.42	288.0
E5	8:05	124.25	27.95	96	19.35	34.49	3.53	94.7
E6	2:05	125.00	27.45	97	20.77	34.53	4.25	-80.5
E7	18:19	125.80	26.87	1136	23.75	34.62	2.18	-91.1
F2	20:37	126.33	31.89	88	18.15	34.30	8.49	-15.4
F3	17:14	126.50	31.30	85	18.05	34.23	8.60	-23.4
F4	12:43	126.85	30.50	91	19.33	34.34	7.80	417.9
F5	7:31	127.25	29.65	123	20.22	34.51	5.77	94.1
F6	1:39	127.60	28.80	1003	23.43	34.45	6.84	-89.4
FJ0	15:01	122.80	31.33	52	14.86	32.65	7.39	-19.9
FJ1	13:37	123.50	31.33	46	16.66	33.95	12.00	183.4
FJ2	7:48	124.50	31.34	50	15.49	32.90	11.19	51.8
FJ3	3:38	125.31	31.32	54	14.66	32.39	7.27	-12.4
FJ5	14:31	122.60	30.10	24	13.69	29.03	8.23	18.8
H1	9:55	122.74	36.97	28	6.35	31.99	9.80	165.8
H10	21:25	123.00	38.75	51	7.36	32.20	3.11	-104.1

H11	2:04	123.80	38.75	51	7.75	32.18	5.58	-62.3
H12	7:15	123.97	39.50	19	2.09	30.79	5.09	-96.3
H13	11:11	123.21	39.29	31	4.77	31.92	4.79	226.7
H2	6:00	123.38	37.00	68	9.16	32.14	9.12	-20.3
H3	2:31	123.97	37.00	74	9.62	32.25	7.94	-85.5
H4	19:04	123.96	38.00	72	8.84	32.20	6.50	-110.0
H5	23:33	123.00	38.00	55	7.90	32.23	4.75	-111.8
H6	4:19	122.05	38.00	46	7.41	32.22	8.39	-107.4
H7	8:47	121.16	38.00	17	6.48	32.26	4.60	25.7
H8	11:12	121.16	38.36	47	7.14	32.24	1.48	236.3
H9	16:37	122.08	38.75	46	4.67	32.16	0.68	-94.6
J1	20:48	122.01	33.00	11	8.64	31.54	4.51	-17.4
J2	15:21	123.01	32.96	28	12.35	31.68	6.82	-14.2
J3	9:58	123.99	33.00	45	13.22	32.42	6.25	71.0
P1	12:15	122.72	30.96	19	13.96	30.61	3.59	22.9
P2	9:53	123.01	30.87	47	15.76	33.04	2.90	14.1
P3	21:31	123.75	30.37	53	17.48	33.96	6.98	-87.4
P4	2:40	124.55	29.85	62	17.61	33.88	8.52	-81.8
P5	8:48	125.39	29.27	87	18.97	34.19	7.49	266.0
P6	14:36	126.15	28.70	121	20.62	34.51	7.17	118.7
P7	20:15	127.00	28.15	899	23.31	34.66	7.32	-75.5
S1	9:55	121.47	27.85	22	14.01	29.78	7.81	222.9
S2	13:05	121.63	27.58	44	17.83	33.90	8.93	266.6
S3	16:37	122.00	27.33	83	19.52	34.34	5.87	-53.6
S4	12:08	122.75	27.15	104	20.42	34.51	5.46	30.7
S5	2:44	123.36	26.65	138	21.05	34.35	4.25	-33.9
S6	8:05	124.2	26.54	140	22.98	34.43	4.80	162.0
T1	0:56	120.51	26.84	22	14.59	29.61	8.69	-33.2
T2	21:12	120.92	26.61	59	17.88	33.15	3.04	-26.6
T3	17:22	121.35	26.30	75	20.12	33.58	4.02	-12.8
T4	13:31	121.77	26.00	117	19.62	34.07	5.98	17.9
T5	6:03	122.67	25.48	659	19.75	34.43	9.44	-9.1

90

Table S2. Spectral characteristics of the three fluorescent components identified by the PARAFAC model in this study, compared with those preciously identified.

Component	E_x: E_m	Tradition peak Coble (2007)	Fluorescence type	Comparison with other studies using PARAFAC
C1	275/335	Peak T:275/340	Tryptophan-like	Tryptophan-like C5: 275/330 (Zhu et al., 2017) Tryptophan protein-like C5: 275/325 (Chari et al., 2012) Tryptophan-like C4: 275/340 (Guo et al., 2014)
C2	350/455	Peak C:320-360/420-460	Terrestrial humic-like	Humic-like C1: 330/425 (Zhu et al., 2017)
C3	320/390	Peak M:290-310/370-410	Marine humic-like	Marine humic-like C3: 250(310)/400 (Kowalczuk et al., 2010) Marine humic-like C1: < 250(310)/416 (Williams et al., 2010) Humic-like C2: 250/420 and C3: 250(310)/400 (Kowalczuk et al., 2010)

Table S3. Production rate and biological consumption rate of CO in the sea surface microlayer and subsurface water of the eastern marginal seas of China and its sea-to-air flux.

Station	Time	Temperature	Salinity	SML		SSW		Wind speed	Flux in the SML	Flux in the SSW	$[CO]_{sur}$
				k_{bio}	k_{photo}	k_{bio}	k_{photo}				
		(°C)		(nmol L^{-1} h^{-1})	(nmol L^{-1} h^{-1})	(nmol L^{-1} h^{-1})	(nmol L^{-1} h^{-1})	(m s^{-1})	(μmol L^{-1} h^{-1})	(μmol L^{-1} h^{-1})	(nmol L^{-1})
A1	5:25	8.3	32.2	0.129		0.106		5.91	1.94	2.38	1.22
B1	22:35	10.1	31.7	0.157	0.91	0.049	0.78	3.15	0.50	1.93	1.51
C4	19:11	12.7	32.8	0.145	1.05	0.118	0.97	7.53	3.05	5.58	1.22
P1	12:15	14.0	30.6		1.09		0.83	3.59	2.89	3.70	1.61
E2	22:22	16.6	33.3	0.110	1.06	0.140	1.05	6.53	1.62	6.46	0.98
F5	7:31	20.2	34.5		1.27		0.83	5.77	-2.61	7.72	1.25
T2	21:12	17.9	33.1	0.114		0.109		3.04	-0.14	2.47	1.05
S6	8:05	23.0	34.4	0.069		0.060		4.80	-1.18	3.72	0.82
P7	20:15	23.0	34.7		0.82		0.71	7.32	3.79	12.45	1.20
Average		16.2	33.0	0.121	1.03	0.097	0.86	5.29	1.10	5.16	1.21

References

Carpenter, J.H., 1964. The Chesapeake Bay Institute technique for the Winkler dissolved oxygen method. Limnol. Oceanogr. 10(1964), 141–143.

Chari, N.V.H.K., Sarma, N.S., Pandi, S.R., Murthy, K.N., 2012. Seasonal and spatial constraints of fluorophores in the midwestern Bay of Bengal by PARAFAC analysis of excitation emission matrix spectra. Estuar. Coast. Shelf. S. 100, 162–171.

Chen, Y., Yang, G., Xia, Q., Wu, G., 2016. Enrichment and characterization of dissolved organic matter in the surface microlayer and subsurface water of the South Yellow Sea. Mar. Chem. 182(Mar. 20), 1–13

Chowdhury, S., 2013. Trihalomethanes in drinking water: Effect of natural organic matter distribution. Water SA 39(1), 1–7.

Helms, J.R., Stubbins, A., Ritchie, J.D., Minor, E.C., Kieber, D.J., Mopper, K., 2008. Absorption spectral slopes and slope ratios as indicators of molecular weight, source, and photobleaching of chromophoric dissolved organic matter. Limnol. Oceanogr. 53(3), 955–969.

Hoge, F.E., Vodacek, A., Blough, N.V., 1993. Inherent optical properties of the ocean: retrieval of the absorption coefficient of chromophoric dissolved organic matter from fluorescence measurements. Limnol. Oceanogr. 38(7), 1394–1402.

Guo, W., Yang, L., Zhai, W., Chen, W., Osburn, C.L., Huang, X., Li, Y., 2014. Runoff‐mediated seasonal oscillation in the dynamics of dissolved organic matter in different branches of a large bifurcated estuary—The Changjiang Estuary. J. Geophys. Res. -Biogeosciences 119 (5), 776–793.

Kowalczuk, P., Cooper, W.J., Durako, M.J., Kahn, A.E., Gonsior, M., Young, H., 2010. Characterization of dissolved organic matter fluorescence in the South Atlantic Bight with use

of PARAFAC model: relationships between fluorescence and its components, absorption coefficients and organic carbon concentrations. Mar. Chem. 118 (1–2), 22–36.

Massicotte, P., Asmala, E., Stedmon, C., Markager, S., 2017. Global distribution of dissolved organic matter along the aquatic continuum: Across rivers, lakes and oceans. Sci. Total. Environ. 609(Dec. 31), 180–191.

Ortega-Retuerta, E., Passow, U., Duarte, C.M., Reche, I., 2009. Effects of ultraviolet B radiation on (not so) transparent exopolymer particles. Biogeosciences 6(12), 3071–3080.

Parsons, T.R., Matia, Y., Lalli, C.M., 1984. A Manual of Chemical and Biological Methods for Seawater Analysis. Pergamon Press, Oxford.

Singh, S., D'Sa, E., Swenson, E., 2010. Seasonal variability in CDOM absorption and fluorescence properties in the Barataria Basin, Louisiana, USA. J. Environ. Sci. 22(10), 1481–1490.

Singh, S., D'Sa, E., Swenson, E., 2010. Seasonal variability in CDOM absorption and fluorescence properties in the Barataria Basin, Louisiana, USA. J. Environ. Sci. 22(10), 1481–1490.

Spencer, R.G., Aiken, G.R., Butler, K.D., Dornblaser, M.M., Striegl, R.G., Hernes, P.J., 2009. Utilizing chromophoric dissolved organic matter measurements to derive export and reactivity of dissolved organic carbon exported to the Arctic Ocean: a case study of the Yukon river, Alaska. Geophys. Res. Lett. 36(6), 141–153.

Stedmon, C.A., Bro, R., 2008. Characterizing dissolved organic matter fluorescence with parallel factor analysis: a tutorial. Limnol. Oceanogr.-methods 6(11), 572–579.

Stedmon, C.A., Markager, S., Tranvik, L., Kronberg, L., Slätis, T., Martinsen, W., 2007. Photochemical production of ammonium and transformation of dissolved organic matter in the Baltic Sea. Mar. Chem. 104(3–4), 227–240.

Weishaar, J.L., Aiken, G.R., Bergamaschi, B.A., Fram, M.S., Fujii, R., Mopper, K., 2003. Evaluation

of specific ultraviolet absorbance as an indicator of the chemical composition and reactivity of dissolved organic carbon. Environ. Sci. Technol. 37(20), 4702–4708.

Williams, C.J., Yamashita, Y., Wilson, H.F., Jaffé, R., Xenopoulos, M.A., 2010. Unraveling the role of land use and microbial activity in shaping dissolved organic matter characteristics in stream ecosystems. Limnol. Oceanogr. 55 (3), 1159–1171.

Zepp, R.G., Sheldon, W.M., Moran, M.A., 2004. Dissolved organic fluorophores in southeastern US coastal waters: correction method for eliminating Rayleigh and Raman scattering peaks in excitation–emission matrices. Mar. Chem. 89(1), 15–36.

Zhu, W. Z., Yang, G., Zhang, H., 2017. Photochemical behavior of dissolved and colloidal organic matter in estuarine and oceanic waters, Sci. Total Environ., 607–608, 214–224.